Electronic Supplementary Material (ESI) for Journal of Materials Chemistry A.

Supporting Information

A Novel Composite Strategy to Build a Sub-zero Temperature Stable Anode for Sodium-ion Batteries

Fangjie Mo,[abc] Zixuan Lian,[b] Bowen Fu,[b] Yun Song,*[b] Pei Wang,[b] Fang Fang,[b] Yong-ning Zhou,[b] Shuming Peng[ac] and Dalin Sun*[b]

[a]Shanghai EBIT Lab Key Laboratory of Nuclear Physics and Ion-beam Application, Institute of Modern Physics, Department of Nuclear Science and Technology, Fudan University, Shanghai 200433, China

[b]Department of Materials Science, Fudan University, Shanghai 200433, China

[c]Key Laboratory for Neutron Physics of Chinese Academy of Engineering Physics, Institute of Nuclear Physics and Chemistry, Mianyang 621999, China

*Corresponding author:

E-mail: songyun@fudan.edu.cn, dlsun@fudan.edu.cn

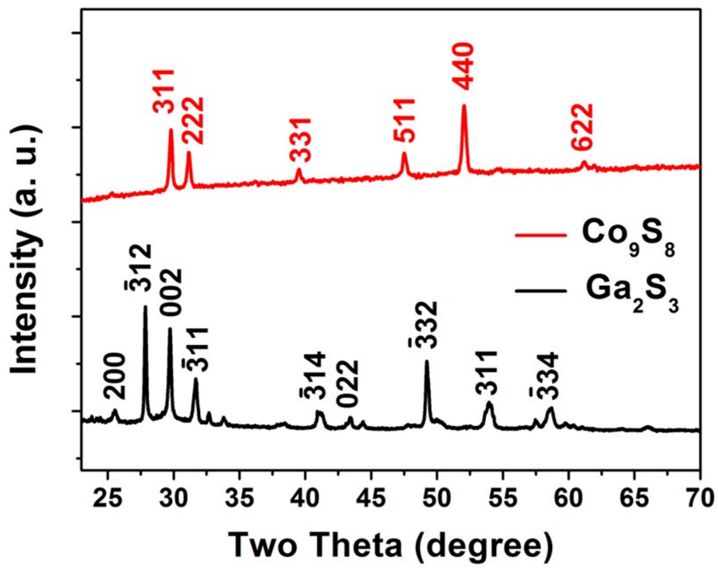

Figure S1. XRD patterns of as-synthesized Co_9S_8 and Ga_2S_3

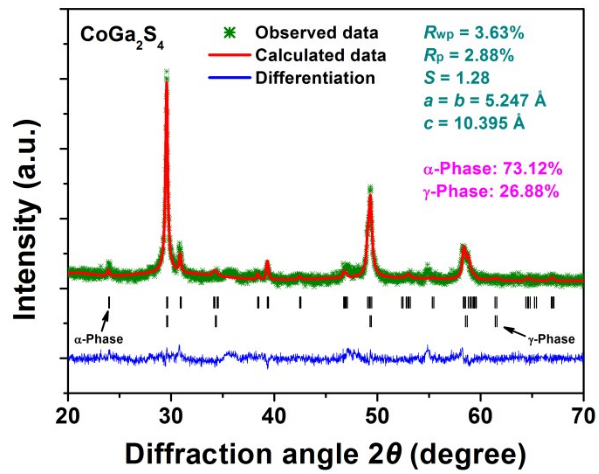

Figure S2. XRD pattern of $CoGa_2S_4$ and the corresponding Rietveld refinement.

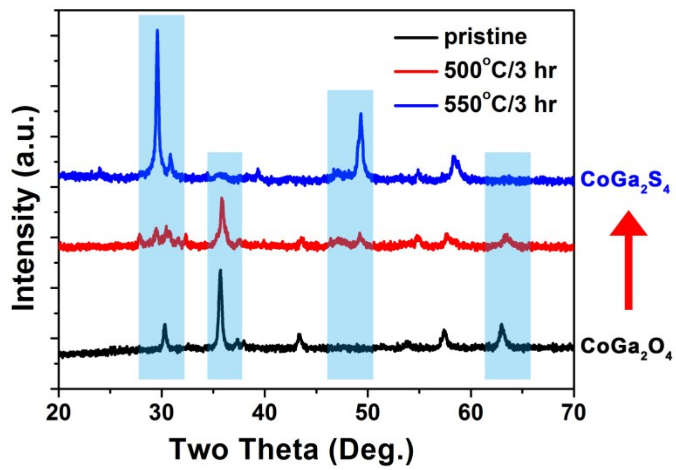

Figure S3. XRD patterns of pristine $CoGa_2O_4$ and the product after sulfided under 500 ºC and 550 ºC, respectively.

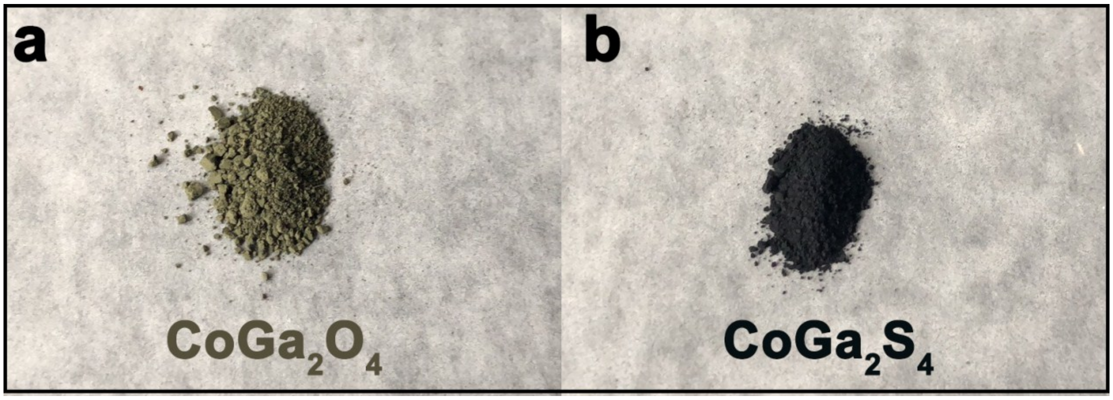

Figure S4. The as-synthesized (a) $CoGa_2O_4$ and (b) $CoGa_2S_4$ powder.

X-ray photoelectron spectroscopy (XPS) analysis: the XPS survey spectrum (Figure S5a) confirms the existence of Co, Ga, S, C and O elements in the $CoGa_2S_4$@G. Co 2p spectrum fits well with two spin-orbit doublets (Figure S5b). Two peaks at 797.7 eV and 793.9 eV attribute to the binding energies of Co^{2+} and Co^{3+} for Co $2p_{1/2}$, respectively, while those arise at 781.8 eV and 778.5 eV are ascribed to the binding energies of Co^{2+} and Co^{3+} for Co $2p_{3/2}$, respectively. Peaks at 802.3 eV and 786.0 eV correspond to the shakeup satellites (noted as 'Sat.'). Figure S5c shows two peaks at 1146.4 eV and 1119.2 eV, which attribute to the spin-orbit characteristics of Ga $2p_{1/2}$ and Ga $2p_{3/2}$, respectively. Two fitting peaks in Figure S5d with binding energies of 163.8 eV and 162.6 eV correspond well to S $2p_{1/2}$ and S $2p_{3/2}$, respectively.

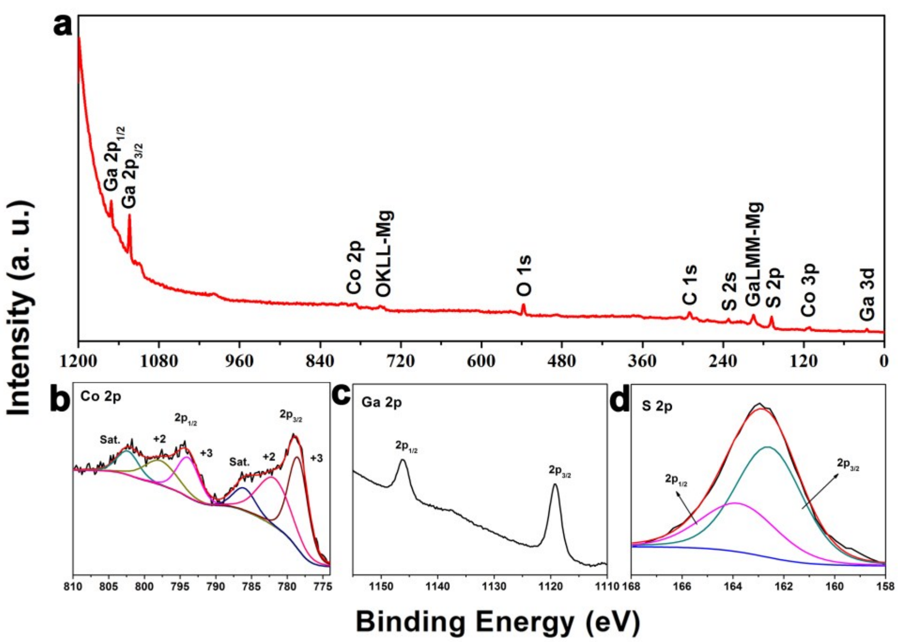

Figure S5. (a)XPS survey spectrum of the $CoGa_2S_4$@G and high resolution XPS spectra of (b) Co 2p, (c) Ga 2p and (d) S 2p.

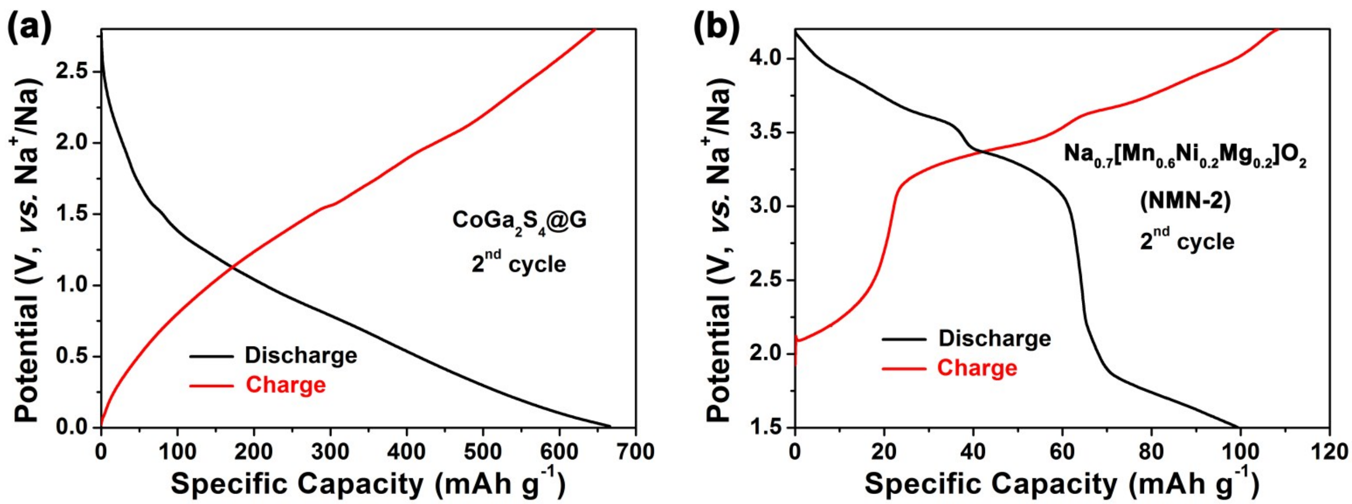

Figure S6. Room temperature GDC profiles for the 2nd cycle of (a) CoGa2S4@G and (b) $Na_{0.7}[Mn_{0.6}Ni_{0.2}Mg_{0.2}]O_2$ (NMN-2) half cells at 0.5 C, respectively.

Freezing resistance test of ether-based sodium ion batteries electrolyte: ~5 mL electrolyte was filled in a glass bottle sealed by black tape in glovebox with ultrahigh pure argon gas. The glass bottle was then put in low temperature test chamber, setting temperature to -60 ºC. After 100 h, the electrolyte in glass bottle still remained liquid.

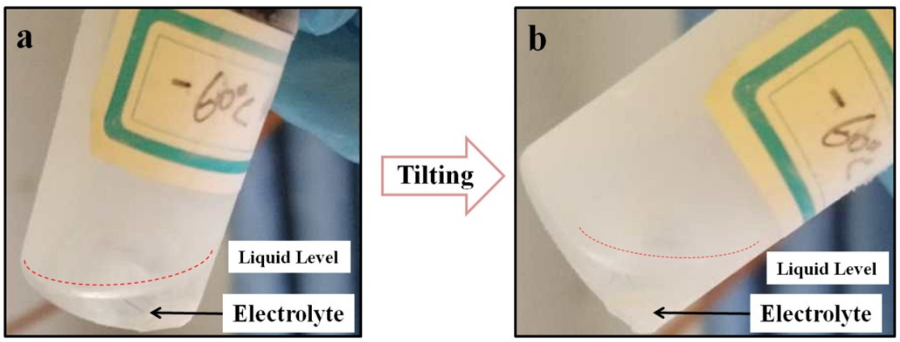

Figure S7. (a) After 100 h at -60 ºC in low temperature test chamber, the glass bottle filled with electrolyte is quickly took out from the chamber, (b) after tilting the glass bottle, electrolyte still shows as well fluidity as that at room temperature.

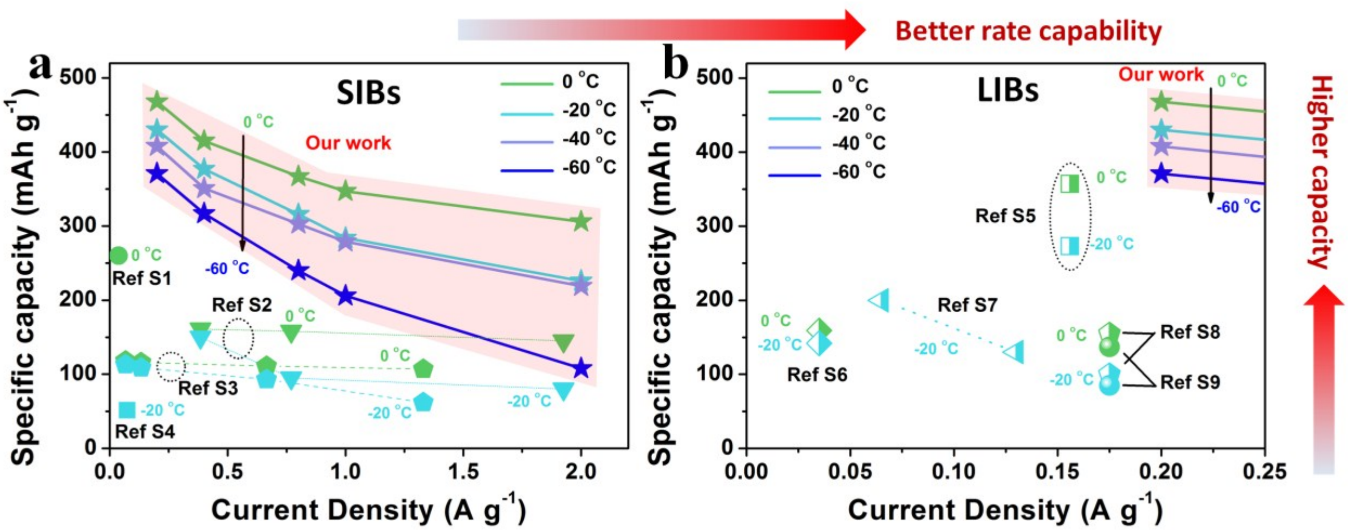

Figure S8. Comparison of rate capability at different temperatures with the reported anodes for (a) SIBs and (b) LIBs.[S1-S9]

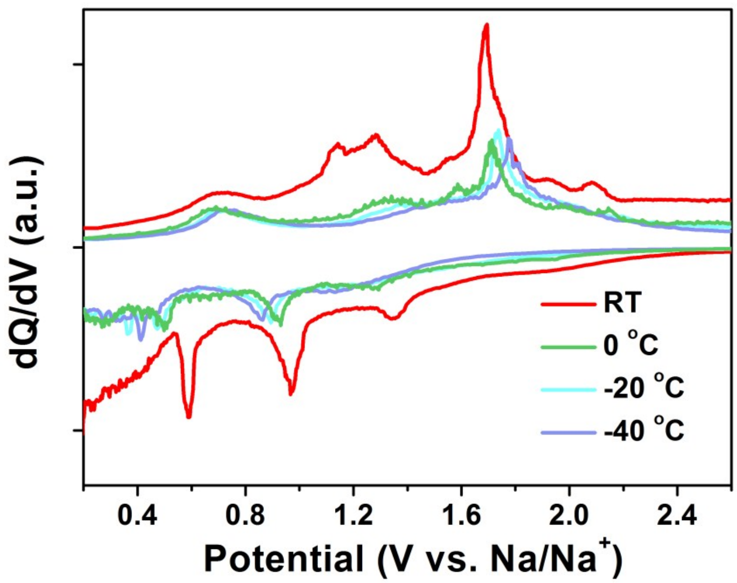

Figure S9. d*Q*/d*V* profiles of GDC curves at 0.2 A g^{-1} for RT, 0 ºC, -20 ºC, -40 ºC, respectively.

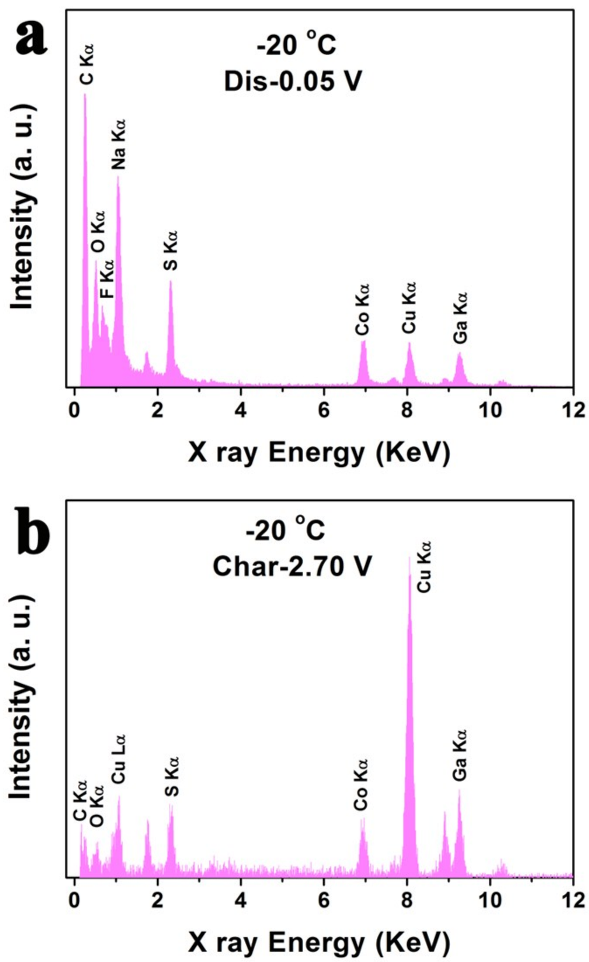

Figure S10. EDX spectrum of the $CoGa_2S_4$@G electrode after (a) discharging to 0.05 V and (b) charging to 2.70 V at -20 ºC, respectively.

References

(S1) Liu,Y.; Yang, B.; Dong, X.; Wang, Y.; Xia, Y. A Simple Prelithiation Strategy To Build a High-Rate and Long-Life Lithium-Ion Battery with Improved Low-Temperature Performance. *Angew. Chem. Int. Ed.* **2017**, *56*, 16606–16610.

(S2) Chen, J.; Fan, X.; Ji, X.; Gao, T.; Hou, S.; Zhou, X.; Wang, L.; Wang, F.; Yang, C.; Chen, L.; Wang, C. Intercalation of Bi Nanoparticles into Graphite Results in an Ultra-Fast and Ultra-Stable Anode Material for Sodium-Ion Batteries. *Energy Environ. Sci.* **2018**, *11*, 1218–1225.

(S3) Wang, L.; Wang, B.; Liu, G.; Liu, T.; Gao, T.; Wang, D. Carbon Nanotube Decorated $NaTi_2(PO_4)_3/C$ Nanocomposite for a High-Rate and Low-Temperature Sodium-Ion Battery Anode. *RSC Adv*. **2016**, *6*, 70277–70283.

(S4) Li, Q.; Jiang, K.; Li, X.; Qiao, Y.; Zhang, X.; He, P.; Guo, S.; Zhou, H. A High-Crystalline $NaV_{1.25}Ti_{0.75}O_4$ Anode for Wide-Temperature Sodium-Ion Battery. *Adv. Energy Mater*. **2018**, *8*, 1801162.

(S5) Nobili, F.; Mancini, M.; Dsoke, S.; Tossici, R.; Marassi, R. Low-Temperature Behavior of Graphite-Tin Composite Anodes for Li-Ion Batteries. *J. Power Sources* **2010**, *195*, 7090–7097.

(S6) Marinaro, M.; Nobili, F.; Birrozzi, A.; Moorthy, S. K. E.; Kaiser, U.; Tossici, R.; Marassi, R. Improved Low-Temperature Electrochemical Performance of $Li_4Ti_5O_{12}$ Composite Anodes for Li-Ion Batteries. *Electrochim. Acta* **2013**, *109*, 207–213.

(S7) Yan, Y.; Ben, L.; Zhan, Y.; Huang, X. Nano-Sn Embedded in Expanded Graphite as Anode for Lithium Ion Batteries with Improved Low Temperature Electrochemical Performance. *Electrochim. Acta* **2016**, *187*, 186–192.

(S8) Zou, H. L.; Xiang, H. F.; Liang, X.; Feng, X. Y.; Cheng, S.; Jin, Y.; Chen, C. H. Electrospun $Li_{3.9}Cr_{0.3}Ti_{4.8}O_{12}$ Nanofibers as Anode Material for High-Rate and Low-Temperature Lithium-Ion Batteries. *J. Alloy Compd.* **2017**, *701*, 99–106.

(S9) Pohjalainen, E.; Rauhala, T.; Valkeapää, M.; Kallioinen, J.; Kallio, T. Effect of $Li_4Ti_5O_{12}$ Particle Size on the Performance of Lithium Ion Battery Electrodes at High C-Rate and Low Temperatures. *J. Phys. Chem. C* **2015**, *119*, 2273–2283.